A&A 526, A115 (2011)
DOI: 10.1051/0004-6361/201016132

Astronomy & Astrophysics

Electron-impact excitation of H-like Cr, Mn, Fe, Co, and Ni for applications in modeling X-ray astrophysical sources⋆

C. Malespin[1], C. P. Ballance[2], M. S. Pindzola[2], M. C. Witthoeft[1], T. R. Kallman[1], and S. D. Loch[2]

[1] NASA Goddard Space Flight Center, Greenbelt, MD 20771, USA
e-mail: Charles.A.Malespin@nasa.gov
[2] Auburn University, Auburn, AL 36849, USA

Received 11 November 2010 / Accepted 29 November 2010

ABSTRACT

Context. Accurate atomic data for the less abundance Fe-peak elements are required for use in X-ray astrophysical studies.
Aims. We calculate high quality electron-impact excitation collision strengths and effective collision strengths for hydrogenic Cr, Mn, Fe, Co, and Ni.
Methods. We use the Dirac *R*-matrix method, the intermediate coupling frame transformation *R*-matrix method, the semi-relativistic distorted-wave method and the fully-relativistic distorted-wave method to calculate collision strengths for each of the ions. The ADAS collisional-radiative codes are used to produce photon emissivity coefficients for each ion.
Results. Results are presented for atomic energy levels, spontaneous emission coefficients, electron-impact excitation collision strengths and associated effective collision strengths for each of the five species under consideration. We find relativistic effects can contribute an approximate 10% increase to the background cross section in relation to semi-relativistic collision calculations. We also confirm that radiation damping plays a prominent role for certain near threshold resonances. In order check the integration of our results within collisional-radiative modeling codes, we have used the ADAS package for some preliminary modeling of photon emissivities. The atomic data shall be made available online through the OPEN-ADAS site and the CFADC database

Key words. atomic data – atomic processes – supernovae: general

1. Introduction

Recent X-ray observations of Fe-peak elements from supernova remnants have highlighted the need for accurate atomic data for highly charged, less abundant Fe-peak elements such as Mn, Cr, Co, and Ni. The first X-ray observation of spectral emission from Co and Mn was reported for the He-like ion stages in the Galactic supernova remnant W49B using observations by the ASCA X-ray satellite (Hwang et al. 2000). These detections were later confirmed by XMM-Newton observations (Miceli et al. 2006). Since no photon emissivity data existed for the He-like stages of Co or Mn, Hwang et al. (2000) estimated emissivities by interpolating the emissivity data generated for Ca, Fe, Ni by the Raymond and Smith thermal models Raymond & Smith 1977; these were then used to infer the abundances of these elements. Subsequently, Cr line emission has been reported for W49B, Tycho's SNR, Kepler's SNR, and Cas A with *Chandra* observations (Yang et al. 2009). Generally the Cr ion states (as estimated by the centroid energy of the Cr emission in these moderate-resolution CCD spectra) track the ion stages of Fe in the same objects and range from an estimated Ne-like to He-like ions. Tamagawa et al. (2009) also used the Suzaku X-ray observatory to tentatively identify the detected Mn and Cr emissions in Tycho's SNR with the Ne-like stage. Mn and Cr emission have now also been reported in the X-ray emission from clusters of galaxies (e.g., Tamura et al. 2010). Aside from their presence in X-ray spectra, the line emission of the Fe-peak elements in supernova remnants are important diagnostics of supernova explosions. For example, the Mn-to-Cr line strengths are sensitive to the neutron excess in Type Ia (thermonuclear) explosions, and are diagnostics of the progenitor metallicity (Badenes et al. 2008). These are important constraints given that we do not yet know the details of the progenitor systems that produce Ia supernovae.

The interpretation of these diagnostics depend on having accurate atomic data for the Fe-peak elements. In this paper we calculate a set of atomic data for H-like Fe peak elements that can be used in analyzing X-ray spectra from these H-like ions. Work on further iso-electronic sequences is currently in progress. In our calculations, we compare with NIST (Ralchenko et al. 2010) level energies and spontaneous emission coefficients for H-like Co, Mn, Fe, Cr and Ni. We also present calculations for electron-impact excitation for each of these ions. In the case of Co, Mn, Cr and Ni these are the first complete *R*-matrix calculations. However, for H-like Fe there have been several previous calculations. Aggarwal & Kingston (1993) performed an *LS* coupling *R*-matrix calculation for all transitions within the first 5 *n*-shells. Radiation damping was shown to be important by Gorczyca and Badnell (1996) in a small $n = 2$ *R*-matrix calculation. Kisielius et al. (1996) performed a fully-relativistic Dirac *R*-matrix calculation for the first 5 *n*-shells, but without radiation damping. Radiation damping was included in the $n = 5$ Breit-Pauli *R*-matrix calculation of Ballance et al. (2002). Recently, a Dirac *R*-matrix calculation by Aggarwal et al. (2008) was performed but without the effects of radiation damping. Aggarwal et al. (2008) reported that for most of the transitions there was

⋆ Final datasets for each ion are only available in electronic form at CDS via anonymous ftp to
cdsarc.u-strasbg.fr (130.79.128.5) or via
http://cdsarc.u-strasbg.fr/viz-bin/qcat?J/A+A/526/A115

reasonable agreement with the results of Ballance et al. (2002), however they saw differences up to 20% on some of the low temperature rate coefficients and even larger differences for a small selection of transitions. Chen et al. (2010) calculated relativistic distorted-wave data using the flexible atomic code (Gu 2003) for the first 6 n-shells, including radiation damping. Effective collision strengths for allowed transitions between nearly degenerate levels for all H-like ions from $Z = 6$ to 30 were calculating using the Coulomb-Born method by Hamada et al. (2010). Although discrepancies exist between these Fe calculations, which we discuss later, it is clear that both radiation damping and a fully-relativistic treatment of the scattering problem are important. Until this work, these two aspects have not been included in the same R-matrix calculation. The main purpose of this paper is to report on new atomic data for H-like Mn, Co, Cr, and Ni using the new Fe data to verify the accuracy of our results. We note that while current astrophysical observations of Mn and Cr are for ion stages less charged than H-like (i.e. He-like and Ne-like), the calculations presented here are with a view to assisting the search and identification of possible H-like lines, and as an initial study with calculations of the ion stages beyond H-like to follow.

To the best of our knowledge experimental measurements for excitation cross sections of H-like Fe-peak elements only exist for H-like Fe. Measurements of the Lyman α_1 excitation cross sections for Fe^{25+} and Ni^{27+} were carried out at the Lawrence Livermore National Laboratory SuperEBIT experiment (Thorn et al. 2009). These measurements were taken at very high electron impact energies beyond our area of interest.

In the next section we describe the theoretical methods used in this study. Section 3 will describe the atomic structure and cross section results. In Sect. 4 we will do some preliminary modeling with the new data and in Sect. 5 we will summarize the results of the work.

2. Calculation methods and details

We use a number of methods to calculate the electron-impact excitation cross sections of H-like Mn, Cr, Fe, Co and Ni. As all of these methods are well described elsewhere, we give here just a brief outline of the various approximations. Our recommended data will come from the fully-relativistic Dirac R-matrix calculations, which we compare with semi-relativistic R-matrix calculations. With both of these R-matrix methods, we calculate results with and without radiation damping. We also compare with semi- and fully-relativistic distorted-wave calculations for the 1s-2s transition in H-like Fe. By comparing these different methods we seek to quantify the importance of using a fully-relativistic treatment and to look at the roles of radiation damping and resonance resolution. The details for each calculation method are presented below.

2.1. Distorted-wave

The configuration-average distorted-wave (CADW) method (Pindzola et al. 1986) has been used with much success to calculate electron-impact excitation cross sections for light species. We generate semi-relativistic energies and bound radial wave functions using Cowan's atomic structure code (Cowan 1981) where the mass-velocity and Darwin corrections have been included. The method can be used to calculate direct excitation cross sections or resonant excitation cross sections. Radiation damping of the resonances can also be included. This method has been used for studies on Fe^{23+} (Pindzola et al. 2002) and on Fe^{16+} (Pindzola et al. 2006).

We also perform fully relativistic, sub-configuration average distorted-wave calculations. In this method, the fully-relativistic energies and bound-radial orbitals are generated using Grant's atomic structure code (Grant 2007). The details of this method can be found in Pindzola et al. (1988) where it was used to calculate the electron-impact ionization of U^{89+} and in Pindzola et al. (1989) for the ionization plus excitation-autoionization of U^{16+}.

2.2. R-matrix

Two R-matrix methods are used in this paper, namely the semi-relativistic intermediate coupling frame transformation (ICFT) method (Griffin et al. 1998) and the relativistic Dirac-Coulomb method (Norrington et al. 1987; Ait-Tahar et al. 1996). The main strength of the ICFT method is that the majority of the calculation is carried out in an LS coupling scheme. Therefore, the formation and diagonalization of the smaller LS resolved Hamiltonians (including mass-velocity and Darwin terms) is less computationally demanding than the associated jK or jJ resolved Hamiltonians. Only in the final stages of the calculation are the term-resolved K matrices transformed into level-to-level collision strengths. For the current study, the ICFT results are used to quantify the importance of having fully-relativistic R-matrix data for H-like systems. We note that it has previously been shown (Griffin et al. 1998 and Munoz Burgos et al. 2009) that the ICFT method gives results that are very close to the Breit-Pauli R-matrix method.

For the ICFT calculations, the hydrogenic 1s-5g orbitals were generated from the atomic structure code AUTOSTRUCTURE (Badnell 1986) resulting in 15 LS terms which were used in our close coupling expansion. The scattering calculation was performed with our set of parallel R-matrix programs (Mitnik et al. 2003; Ballance et al. 2004), which are extensively modified versions of the serial RMATRIX I programs (Berrington et al. 1995). A basis of 70 continuum functions was used to span the energy range from the ground state to four times the ionization threshold for each of the hydrogenic systems under consideration. In the scattering calculation, 50 partial waves ranging over angular momenta $L = 0$–12 were employed in the exchange scattering calculation. A further 162 higher partial waves, $L = 13$–50, were also calculated where exchange effects were neglected. The results were then topped up at higher L using the method described by Burgess (1970) for dipole transitions and a geometric series for non-dipole transitions. AUTOSTRUCTURE was used to calculate infinite-energy Bethe/Born limit points using our semi-relativistic structure to allow us to interpolate our collision strengths to higher energies.

For the Dirac R-matrix calculations, we obtained our target orbitals, energy levels and radiative rates using the multi-configuration Dirac-Fock (MCDF) atomic structure program GRASP0 (Dyal et al. 1989; Parpia et al. 1996). The resulting 25 relativistic orbitals produced 25 Jπ levels, all of which were used in our close-coupling expansion. For the scattering calculation we used a recently parallelized version of the Dirac Atomic R-matrix Codes (DARC) (Ballance et al. 2006) which are based on portions of DARC from Norrington et al. (1987) and Ait-Tahar et al. (1996). In the DARC calculations, full exchange effects were included for $J = 0$–11 and neglected for $J = 12$–50. Higher partial wave results were then approximated using the same top-up procedure described above (Burgess 1970). As these results shall be our recommended data sets for use in plasma modeling, the energy levels were shifted slightly to

match NIST spectroscopic values. Given the highly charged nature of the five hydrogenic species under consideration, radiation damping will affect the resonance contribution to the cross sections and the subsequent Maxwellian-averaged rates based upon them. Both R-matrix calculations implement radiation damping of resonances as described in Robicheaux et al. (1995). It is important that the resonance structure be carefully resolved over the entire energy range. Therefore, in order to make meaningful comparisons between the two R-matrix methods, a very fine energy mesh of 400 000 points from the first to the last threshold was used for both the ICFT and DARC calculations.

The R-matrix calculations provide dimensionless collision strengths for all transitions between the levels of the target ion. For modeling purposes, Maxwellian excitation rate coefficients are required which can be expressed in terms of effective collision strengths. The effective collision strengths (Υ) are obtained by convolving the collision strengths with a Maxwellian electron distribution. Burgess-Tully plots (Burgess Tully 1992) are used to show effective collision strengths versus a scaled energy from threshold to the infinite-energy limit on a scale from zero to one. For the type 2 (non-dipole, non-spin-changing) transitions that we will consider (1s–2s), this involves the following transformations:

$$X = \frac{\frac{kT}{E_{ij}}}{\frac{kT}{E_{ij}} + C} \quad (1)$$

$$Y = \Upsilon_{ij} \quad (2)$$

where E_{ij} is the energy of the transition i to j, and C is an arbitrary constant, for which we will use a value of 0.5.

2.3. Collisional-radiative modeling

As well as archiving our fundamental atomic collision data, we also archive a set of photon emissivity coefficients (PECs) produced from a collisional-radiative model. These PECs can be used in direct comparison with an observed spectrum. They also serve as an illustration of how the new data can be used in collisional-radiative modeling of X-ray sources.

To produce photon emissivity coefficients for each element in our study, we use collisional-radiative theory (Bates et al. 1962) as implemented in the ADAS suite of codes (http://www.adas.ac.uk), see Summers et al. (2006) for more details on the method. The photon emissivity coefficients for a given transition $j \rightarrow k$, which include collisional and radiative redistribution between the excited states (i and j) are given by

$$\mathrm{PEC}^{\mathrm{exc}}_{j\rightarrow k} = A_{j\rightarrow k} \sum_i C^{-1}_{ji} C_{i1} \quad (3)$$

$$\mathrm{PEC}^{\mathrm{rec}}_{j\rightarrow k} = A_{j\rightarrow k} \sum_i C^{-1}_{ji} R_{i+} \quad (4)$$

where $A_{j\rightarrow k}$ is the spontaneous emission coefficient for the transition $j \rightarrow k$ and the C-matrix elements contain the collisional and radiative rates connecting the excited levels of the atom. C_{i1} is the excitation rate coefficient from the ground of the H-like ion to level i and R_{i+} is the total recombition rate coefficient from the ground of the fully stripped ion into level i of the H-like ion. For most plasma applications the $\mathrm{PEC}^{\mathrm{exc}}$ dominates the line emission. The temperature- and density-dependent photon emissivity coefficients for transition $j \rightarrow k$ are in units of photons cm^3 s^{-1}. When each of these coefficients is multiplied by the electron density and the density of the relevant ground state ion density, the result is the number of photons emitted per unit volume per unit time. For $\mathrm{PEC}^{\mathrm{exc}}$ the relevant ground population is the ground of the H-like ion stage and for $\mathrm{PEC}^{\mathrm{rec}}$ the relevant driving population is that of the bare ion. We archive PEC coefficients for the 50 strongest transitions for each ion on a temperature-density grid. These can then be used for direct comparison with spectral observations.

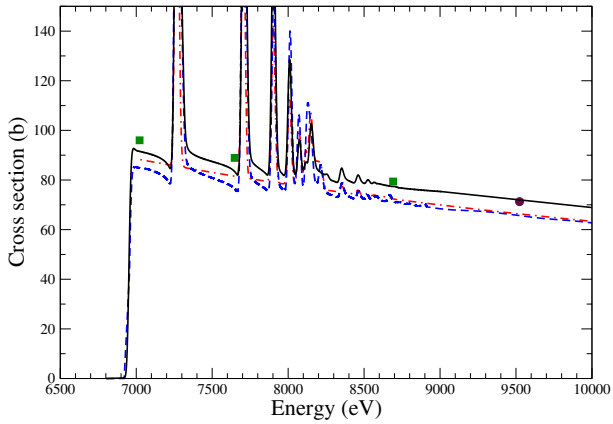

Fig. 1. Electron impact excitation cross section for the 1s–2s transition in H-like Fe. The cross sections have been convolved with a 25 eV $FWHM$ Gaussian distribution. The solid line shows the DARC results with radiation damping included, the dashed line show the ICFT results with radiation damping included. The dot-dashed line shows the semi-relativistic CADW results with radiation damping included. The solid squares show the direct excitation calculated using a fully-relativistic distorted-wave method. The solid circles show the DARC calculation of Aggarwal et al. (2008).

3. Results and discussion

We used both AUTOSTRUCTURE (Badnell 1986) and the GRASP0 multi-configuration Dirac-Fock code (Dyal et al. 1989; Parpia et al. 1996) to provide our atomic structure. As expected for hydrogenic systems, the calculated level energies were very close to NIST values with an average difference of 0.05% for each of the ions. However, since the relativistic calculations (GRASP0, DARC) are to form the basis of our recommended data set, before the diagonalization of Hamiltonians representing our partial wave expansion we shifted our GRASP0 calculated energies to experimental spectroscopic NIST values. The relativistic spontaneous emission coefficients calculated from our DARC calculations for the 5 species under consideration here were within 2% of the available NIST values.

For our collision calculations, a number of systematic checks on Fe^{25+} were performed to investigate differences between existing datasets in the literature. Our first conclusion is that the fully relativistic R-matrix results show an increase in the background excitation cross section of about 10% compared with the semi-relativistic R-matrix results. This is not entirely surprising given the relativistic nature of the atomic structure of these H-like ions. A 1s orbital for atomic systems ranging from 23 to 27 times ionized should exhibit relativistic effects. Indeed, the Einstein A coefficient from the AUTOSTRUCTURE calculation was approximately 10% less than the Dirac-Fock value from GRASP0 for the $1s_{1/2} \rightarrow 2s_{1/2}$ transition in Fe^{25+}. Figure 1 shows the difference in the semi- and fully-relativistic excitation cross sections for the 1s-2s tranistion in Fe^{25+}, with the background of the ICFT being about 10% below the DARC results. This result is confirmed with semi- and fully-relativistic distorted-wave calculations for the 1s–2s excitation, also shown

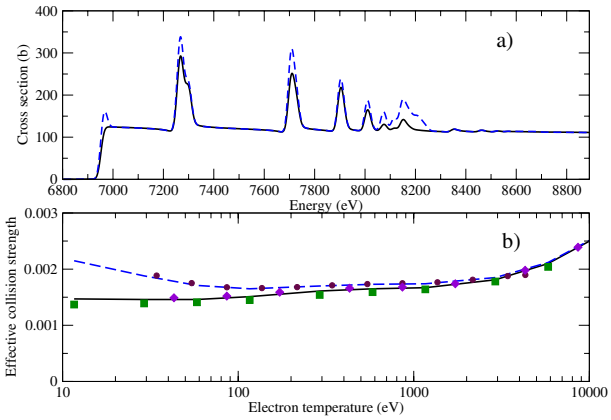

Fig. 2. Electron impact excitation cross section for the $1s_{1/2}$–$2p_{1/2}$ transition in H-like Fe. In **a)** the solid line shows the DARC results with damping included, the dashed line shows the DARC results without radiation damping. The cross sections have been convolved with a 25 eV *FWHM* Gaussian distribution. In **b)** the solid line shows the DARC effective collision strengths with radiation damping included, the dashed lines show the DARC results without radiation damping. The solid circles are the DARC results of Aggarwal et al. (2008) and the solid squares are the ICFT results (with radiation damping) calculated as part of this work. The solid diamonds show the damped FAC calculations of Chen et al. (2010).

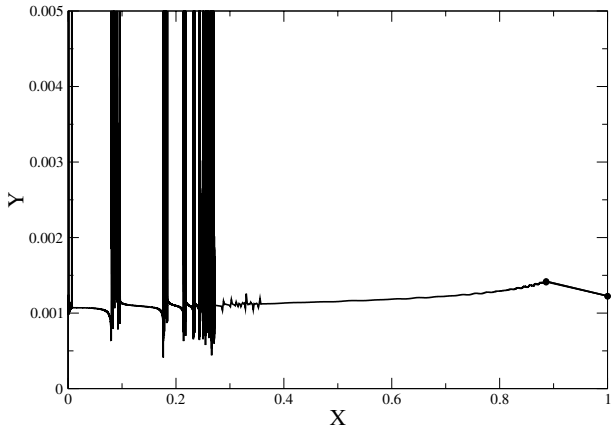

Fig. 3. Electron impact excitation cross sections for the 1s–2s transition in H-like Fe. The results of the damped DARC calculation are shown on a Burgess-Tully plot with $C = 0.5$. The solid circles show the last finite energy point and the infinite energy point.

in Fig. 1. The semi-relativistic distorted-wave results include both direct and resonant excitation and are very close to the ICFT results. The fully relativistic sub-configuration average distorted-wave direct excitation cross section results are in good agreement with the background of the DARC results. We note that this 10% difference is seen in all excitations from the 1s subshell, and in the 1s transitions for the others members of the H-like Fe-peak. This difference presumably decreases as one moves to less ionized ion stages. The close agreement of the distorted-wave and *R*-matrix results shown in Fig. 1 indicates that a fully-relativistic distorted-wave calculation which includes resonant excitation would provide accurate excitation data for these Fe-peak elements. This is investigated in detail by Chen et al. (2010), who compare fully relativistic distorted-wave results using the FAC code (Gu 2003) with the DARC calculations of Aggarwal et al. (2008) and the ICFT calculations of Ballance et al. (2002). They report both damped and undamped FAC effective collision strengths, with the undamped FAC results being very close to the undamped DARC calculation of Aggarwal et al.(2008), showing the similarity of perturbative and non-perturbative calculations for such a highly charged system.

Our study also confirms the earlier conclusions of Gorczyca and Badnell (1996), that the low energy resonances are significantly reduced by radiation damping. It is well known that low temperature Maxwellian-averaged collision strengths are very sensitive to the position and magnitudes of near threshold resonances, and therefore to radiation damping that effects these magnitudes. Figure 2 shows a comparison for the $1s_{1/2} \rightarrow 2p_{1/2}$ transition for Fe^{25+}. Figure 2a shows the DARC cross section results with and without radiation damping. Note that the resonances just above threshold are almost completely damped out. These high n resonances are attached to the $2s_{1/2}$ and $2p_{3/2}$ thresholds. The strong radiative decay of the 2p electron effectively damps out these resonances. Furthermore, there is also noticeable damping of the $3l3l'$, $3l4l'$ resonances between the $n = 2$ and $n = 3$ thresholds, however this does not have as strong an effect on the Maxwellian averaged rate coefficients as the damping of the near threshold resonances. We note that the sensitivity of effective collision strengths to near threshold resonances was also noted by Chen et al. (2010) in their FAC calculations of Fe^{25+}. Indeed, their damped FAC results shown on Fig. 2 are in good agreement with our damped DARC calculation over the entire energy and temperature range of the plots. Comparing the Maxwellian effective collision strengths (Fig. 2b) one can see that the radiationally damped rate coefficients for the $1s_{1/2} \rightarrow 2p_{1/2}$ differ from non-damped results by 10% at 116 eV (1.35×10^6 K), with this difference reducing as the temperature increases. By 5748 eV (6.67×10^7 K) the difference is about 1%. Similar results were seen for the other excitations from the 1s subshell in Fe^{25+}, and for the same transitions in the other ions. Thus, our final DARC calculations for each ion include radiation damping of the resonances.

Our last calculated incident electron energy of approximately four times the ionization threshold was determined from a series of calculations to progressively higher energies, each of which was then extrapolated to the infinite limit Bethe/Born limits. The limit points for the dipole excitations were calculated as part of the DARC calculations, while the non-dipole limit points were taken from AUTOSTRUCTURE calculations. Care must be taken to ensure that the cross section is approaching its asymptotic limit sufficiently before extrapolating to the infinite limit point, or there is a danger of grossly underestimating/overestimating the Maxwellian averaged rate coefficient. We carried out a series of calculations, extrapolating from progressively higher energies, checking the results on Burgess-Tully plots (Burgess Tully 1992) until the Maxwellian averaged rates converged to a consistent set of rates. Figure 3 shows the 1s–2s reduced effective collision strength on a Burgess-Tully plot, with the last calculated energy (at four times the ionization potential) and the infinite energy points shown. We note that the effective collision strengths shown in Fig. 3, even at the last explicitly calculated energy has still to turn over towards the limit point, but that the difference in the effective collision strength was relatively small for the highest calculated temperature. As a consequence of the large energy span of our DARC calculation, we had to include a large basis set size (70) and a large number of partial waves (up to $J = 50$) in our DARC collision calculations. We note that Chen et al. (2010) also investigated the high energy behaviour of the collision strengths, and included

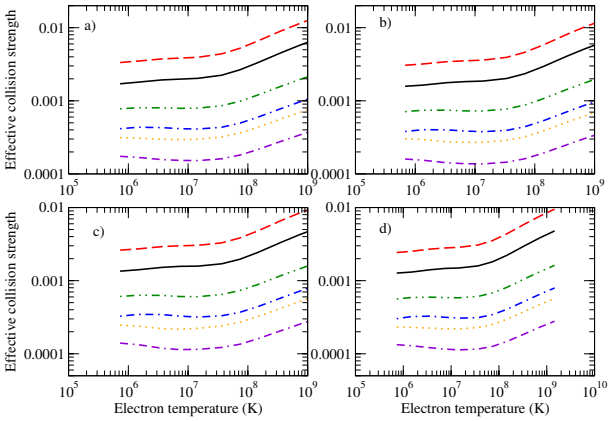

Fig. 4. Effective collision strengths for **a)** Cr, **b)** Mn, **c)** Co and d) Ni. The solid lines show the 1s → $2p_{1/2}$, the dashed lines show the 1s → $2p_{3/2}$, the dot-dashed lines show the 1s → $3p_{1/2}$, the double-dotted dashed lines show the 1s → $3p_{3/2}$, the double-dashed dotted lines show the 1s → $4p_{1/2}$, the dotted lines show the 1s → $4p_{3/2}$ transitions.

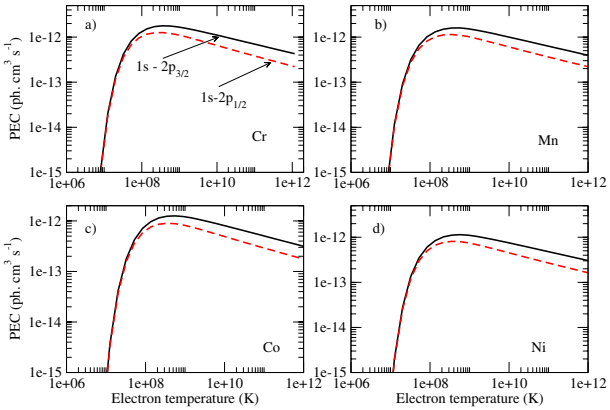

Fig. 5. Photon emissivity coefficients for the 1s → $2p_{3/2}$ (solid line) and the 1s → $2p_{1/2}$ (dashed line) as a function of electron temperature. **a)** for Cr; **b)** for Mn; **c)** for Co; and **d)** is for Ni.

relativistic limit points in both their dipole and non-dipole transitions.

Finally, we looked at the convergence of the excitation rate coefficients with the energy mesh used to resolve the resonance region of the calculation. We progressively doubled the mesh used in this region, and generated effective collision strengths each time. We found that the resonances were extremely narrow. With 400 000 energy mesh points in the resonance region we achieved rate coefficients that were converged to better than 1% for all transitions from the ground. Thus, our final set of calculations for each of the H-like ions consisted of a DARC calculation including radiation damping, using 400,000 energy mesh points in the resonance region. Note that we archive both the level-resolved data and a bundled-*n* version of the data, where the data has been reduced to *n*-shell resolution, see Summers et al. (2006) for more details.

With these convergence checks complete for Fe^{25+}, we generated DARC excitation data based on GRASP0 atomic structure calculations for Mn, Cr, Co and Ni. In the DARC calculations we used the same basis set size, partial wave expansion and energy mesh resolution as in the Fe^{25+} calculation. We also generated undamped DARC and damped/undamped ICFT collision strengths for each ion. Comparing the ICFT with DARC results, there were similar 10% differences in the background cross sections, as seen in Fig. 1. The effect of radiation damping was also similar to that found in Fe^{25+}. Thus, our final recommended data for H-like Mn, Cr, Co and Ni consisted of radiatively damped DARC calculations. The main purpose of this paper is to report on this new data, with this being the first calculations for these ions. The availability of a large amount of data in the literature for H-like Fe allows us to investigate all of the issues mentioned above, with the likelihood that the other Fe-peak elements will behave similarly. Fig. 4 shows a sample of the level-resolved effective collision strength results for Cr, Mn, Co and Ni. Our final datasets for each ion are stored in ADAS adf04 file format (`http://www.adas.ac.uk`), and are available for download via the OPEN-ADAS web site (`http://open.adas.ac.uk`) or via the CFADC web archive (`http://www-cfadc.phy.ornl.gov/data_and_codes/home.html`). The data is also been imported into the ATOMDB database used by the XSPEC modeling codes.

4. Modeling results

For use in spectral modeling, and as an illustration of how the atomic data can be used, we generated a set of photon emissivity coefficients for each of the H-like Fe-peak element ions considered here. An absolute line intensity for the transition is generated by multiplying each PEC by the electron density and by the ground population (for PEC^{exc} this is the ground population of the H-like ion stage and for for PEC^{rec} this is the bare ion density). These ground populations can be evaluated from an ionization balance calculation. For conditions where the excited states are driven primarily from excitation and not from recombination, the ratio of PEC^{exc} for the two transitions will give the predicted line intensity ratio.

We show a sample of the results in Figs. 5 and 6. We first show the photon emissivity coefficients for both 1s-2p transitions for Cr, Mn, Co and Ni. For cases with sufficient electron density, one can get collisional mixing of the 2p and 2s populations. However, our initial collisional-radiative modeling indicates that this does not start to occur until about $N_e = 1 \times 10^{10}$ cm^{-3}. Thus for most supernova remnant studies (where the electron density is typically 1 cm^{-3}), the Lyman α emission will be coming from the sum of the two 2p transitions from the ground. In the limit of higher densities, collisions will drive the 2s and 2p populations to be statistical, relative to each other. This does not happen until about $N_e = 1 \times 10^{24}$ cm^{-3} if electron collisions are the only collisional mixing process, though we note that proton collisions can mix the subshells much more efficiently than electron collisions. For cases where the subshells are strongly collisionally mixed, then the bundled-*n* data is more appropriate. For intermediate densities one needs to do a density-dependent collisional-radiative calculation to calculate the expected line intensities.

As a further illustration of the use of the new data, we show in Fig. 6 the expected Lyman-α to Lyman-β line intensity ratio for Cr, Mn, Co and Ni, for the low density case (Ne $< 1 \times 10^{10}$ cm^{-3}). Thus, if one sees Lyman-α emission from one of these ions, then the plotted results would allow one to determine whether the Lyman-β could be observed, or if it would be buried in the background noise of the spectrum. For example, at $T = 1 \times 10^7$ K, the Lyman-β intensity would be down by an order of magnitude from the Lyman-α intensity for all of the ions studied. Also, as one might expect, the ratio of the Lyman-α to Lyman-β is clearly strongly temperature dependent at the lowest temperatures.

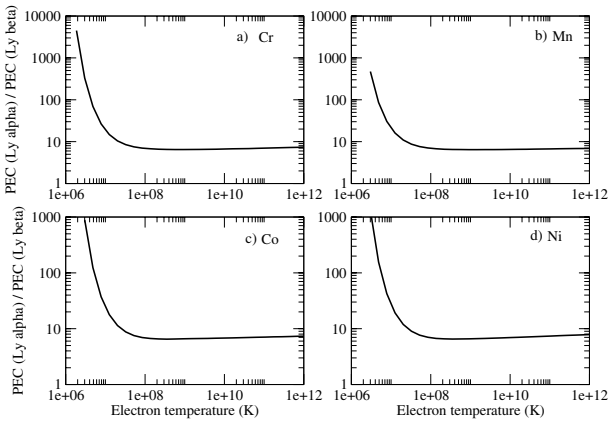

Fig. 6. Lyman α to Lyman β line intensity ratio as a function of electron temperature. Fig. **a)** is for Cr, Fig.**b)** is for Mn, Fig. **c)** is for Co and Fig. **d)** is for Ni.

5. Conclusions

1. Results of electron-impact collision calculations for H-like Cr, Mn, Fe, Co and Ni are presented.
2. Fully relativistic effects results in an approximately 10% rise in the background cross section for the excitations from the ground.
3. Radiation damping must be included for accurate low temperature rate coefficients, and a fine energy mesh is required to resolve all of the resonant structure.
4. Photon emisivity coefficients have been generated on a T_e/N_e grid for H-like Cr, Mn, Fe, Co and Ni.
5. The new atomic data is archived online at the OPEN-ADAS web site (http://open.adas.ac.uk) and the CFADC web archive (http://www-cfadc.phy.ornl.gov/data_and_codes/home.html).
6. Future work will include similar calculations for the He-like stages of these same elements.

Acknowledgements. This work was supported by NASA ROSES ADAP grant NNX10AD46G. The computational work was carried out on the Alabama supercomputer and on the NERSC facilities in California. We would like to thank Una Hwang for the many useful discussions and help that she provided throughout the project.

References

Ait-Tahar, S., Grant, I. P., & Norrington, P. H. 1996, J. Phys. B, 54, 3984
Aggarwal, K. M., & Kingston, A. E. 1993, ApJS, 85, 187
Aggarwal, K. M., Hamada, K., Igarashi, A., et al. 2008, A&A, 484, 879
Badenes, C., Borkowski, K. J., Hughes, J. P., Hwang, U., & Bravo, E. 2006, ApJ, 645, 1373
Badenes, C., Bravo, E., & Hughes, J. P. 2008, ApJ, 680, L33
Badnell, N. R. 1986, J. Phys. B, 19, 3827
Badnell, N. R., & Griffin, D. C. 2001, J. Phys. B, 34, 681
Ballance, C. P., & Griffin, D. C. 2004, J. Phys. B. 37, 2943
Ballance, C. P., & Griffin, D. C. 2006, J. Phys. B, 39, 3617
Ballance, C. P., Badnell, N. R., & Berrington, K. A. 2002, J. Phys. B, 35, 1095
Bates, D. R., Kingston, A. E., & McWhirter, R. W. P. 1962, Proc. Royal Soc. London., 267, 297
Berrington, K. A., Eissner, W. B., & Norrington, P. H. 1995, Comput. Phys. Commun., 92, 290
Burgess, A. 1970, J. Phys. B, 7, L364
Burgess, A., & Tully, J. A. 1992, A&A, 254, 436
Burrows, D. N., Michael, E., Hwang, U., et al. 2000, ApJ, 543, L149
Ciotti, L., D'Ercole, A., Pellegrini, S., & Renzini, A. 1991, ApJ, 376, 380
Chen, C.-Y., Wang, K., Huang, M., Wang, Y.-S., & Zou, Ya-M 2010, J. Quant. Spectr. Radiat. Transf., 111, 843
Colgate, S. A. 1979, ApJ, 232, 404
Cowan, R. D. 1981, The Theory of Atomic Structure and Spectra, (U. Calif. Press, Berkeley)
Dyall, K. G., Grant, I. P., Johnson, C. T., Parpia, F. A., & Plummer, E. P. 1989, Comput. Phys. Commun., 55, 425
Ferrara, A., & Tolstoy, E. 2000, MNRAS, 313, 291
Freedman, W. L., Madore, B. F., Gibson, B. K., et al. 2001, ApJ, 553, 47
Gorczyca, T. W., & Badnell, N. R. 1996, J. Phys. B. 29, L283
Grant, I. P. 2007, Relativistic quantum theory of atoms and molecules (Springer)
Griffin, D. C., Badnell, N. R., & Pindzola, M. S. 1998, J. Phys. B., 31, 3713
Gu, M. F. 2003, ApJ, 582, 1241
Hamada, K., Aggarwal, K. M., Akita, K., et al. 2010, Atom. Data Nucl. Data Tables, 96, 481
Hwang, U., Petre, R., & Hughes, J. P. 2000, ApJ, 532, 970
Hummer, D. G., Berrington, K. A., Eissner, W., et al. 1993, A&A, 279, 298
Immler, S., Brown, P. J., Milne, P., et al. 2006, ApJ, 648, L119
Kisielius, R., Berrington, K. A., Norrington, P. A. 1996, A&A, 118, 157
Miceli, M., Decourchelle, A., Ballet, J., et al. 2006, A&A, 453, 567
Mitnik, D. M., Griffin, D. C., Ballance, C. P., & Badnell, N. R. 2003, J. Phys. B., 36, 717
Munoz Burgoss, M. B., Loch, S. D., Ballance, C. P., & Boivin, R. F. 2009, A&A, 500, 1253
Norrington, P. H., & Grant, I. P. 1987, J. Phys. B., 20, 4869
Parpia, F. A., Froese Fischer, C., Grant, I. P. 1996, Comput. Phys. Commun., 94, 249
Pindzola, M. S. 2002, Phys. Rev. A., 65, 014701
Pindzola, M. S., & Buie, M. J. 1988, Phys. Rev. A., 37, 3232
Pindzola, M. S., & Buie, M. J. 1989, Phys. Rev. A., 39, 1029
Pindzola, M. S., Griffin, D. C., & Bottcher, C. 1986, NATO ASI Series B: Physics, 145, 75
Pindzola, M. S., Loch, S. D., Ballance, C. P., & Griffin, D. C. 2006, Phys. Rev. A., 73, 012718
Raymond, J. C., & Smith, B. W. 1977, ApJS, 35, 419
Ralchenko, Yu., Kramida, A. E., Reader, J., & NIST ASD Team 2008, NIST Atomic Spectra Database (version 3.1.5), Available: http://physics.nist.gov/asd3 [2010, April 4]. National Institute of Standards and Technology, Gaithersburg, MD
Riess, A .G., et al. 1999, ApJ, 116, 1009
Robicheaux, R., Gorczyca, T. W., Pindzola, M. S., & Badnell, N. R. 1995, Phys. Rev. A., 52, 1319
Saha, A., Sandage, A., Tammann, C. A., et al. 1999, ApJ, 552, 802
Summers, H. P., Dickson, W. J., & O'Mullane, M. G. 2006, Plasma Physics and Controlled Fusion, 48, 263
Tamagawa, T., Hayato, A., Nakamura, S., et al. 2009, PASJ, 61, S167
Tamura, T. 2010, BAAS, 41, 703
Thorn, D. B., Beiersdorfer, P., Brown, G. V., et al. 2009, J. Phys.: Conf. Ser., 163, 012036
Yang, X. J., Tsunemi, H., Lu, F. J., & Chen, L. 2009, ApJ, 692, 894